Biosensors and Bioelectronics 133 (2019) 154–159

Contents lists available at ScienceDirect

Biosensors and Bioelectronics

journal homepage: www.elsevier.com/locate/bios

A novel ultrasensitive electrochemiluminescence biosensor for glutathione detection based on poly-L-lysine as co-reactant and graphene-based poly (luminol/aniline) as nanoprobes

Caixia Wang[a,b], Liming Chen[a,b], Peijin Wang[b], Mengsi Li[a,b], Defang Liu[a,b,*]

[a] Key Laboratory of Applied Chemistry of Chongqing Municipality, Institute of Bioorganic and Medicinal Chemistry, Southwest University, 400715, China
[b] School of Chemistry and Chemical Engineering, Southwest University, Chongqing 400715, China

ARTICLE INFO

Keywords:
Electrochemiluminescence
Poly-L-lysine
Glutathione
Co-reactant
Quenching effect

ABSTRACT

In this work, an ultrasensitive electrochemiluminescence (ECL) biosensor was constructed using poly-L-lysine (PLL) as a novel co-reactant of luminol and poly(luminol/aniline) nanorods loaded reduced graphene oxide (PLA@rGO) as nanoprobe, which enable highly sensitivity detection of glutathione (GSH). To the best of our knowledge, it is the first time that PLL was used for the co-reactant of luminol. Notably, about a 5-fold enhancement was obtained compared with the individual PLA@rGO using GCE. Due to the remarkable quenching effect between the excited state of PLL and the reduced form of GSH in the ECL system of luminol/PLL, the ECL sensing platform exhibited wide linear ranges of 1.0×10^{-9}–1.0×10^{-4} M and 1.0×10^{-4}–1.0×10^{-2} M and a low detection limit of 7.7×10^{-10} M. Simultaneously, the biosensor was also successfully applied to detect GSH in human serum sample with high recoveries. Hence, this work would open a new platform for the wide application of PLL in immunoassay and various sensors.

1. Introduction

Glutathione (L-γ-glutamyl-L-cysteinylglycine, GSH), a thiolated tripeptide with multiple physiological functions and medical value (Deng et al., 2011; Stamler and Slivka, 1996; Yin et al., 2014), is widely distributed in a living being system. As one of crucial endogenous antioxidant, scavenger of free radicals, and detoxifying substance, GSH play a key role in immune regulation, human metabolism, energy transport, and other physiological processes (Peng et al., 2018). Abnormal levels of GSH concentration are correlated with various clinical diseases, such as Alzheimer's disease, Parkinson's disease, liver damage, diabetes, epilepsy, atherosclerosis, arthritis, aging, and numerous types of cancers (Harfield et al., 2012). By now, much effort has been made to develop efficient methods for the detection of GSH, including colorimetric (Liu et al., 2017), fluorescent (Fan et al., 2017), electrochemical (Safavi et al., 2009; Wang et al., 2018a), surface enhanced Raman scattering (Wang et al., 2016). However, some drawbacks such as low sensitivity, high cost, intricate test step, costly technical equipment and time-consuming still exist. Thus, to develop a simple, rapid, and sensitive method for monitoring changes of GSH concentrations has important clinical significance.

Electrochemiluminescence, also named electrogenerated chemiluminescence (ECL), Due to its marked features such as sensitivity, wide dynamic range, simplicity, stability and facility (Li et al., 2017), has attracted much attention. Recently, luminol/H_2O_2 ECL systems has been studied widely in many fields including diagnostic, clinical, pharmaceutical, environmental and food analysis (Haghighi and Bozorgzadeh, 2011; Liu et al., 2015; Xu et al., 2013; Sun et al., 2018) because of its low price, high emission yields and low oxidation potential. Nevertheless, H_2O_2 is unstable and easily decomposes in the presence of metal ions or reductants, making the ECL sensor poor selectivity and limiting its application in biological detection (Cao et al., 2012). Thus, it is very important to choose a more stable co-reactant than H_2O_2 in ECL detection. Xu et al. have designed a great method to markedly enhance ECL intensity of luminol by adding tripropylamine (TPA) into working solution as co-reactants (Hanif et al., 2016). However, TPA has some disadvantages such as toxicity and low biological compatibility. Therefore, to search for a suitable co-reactant with low toxicity and good biological compatibility that can enhance the signal of $Ru(bpy)_3^{2+}$ more than TPA is the most important points (Liao et al., 2013). Yuan et al. have designed a reagentless ECL immunesensor using PLL as co-reactant to enhance the ECL of $Ru(bpy)_3^{2+}$ for the detection

* Corresponding author at: Key Laboratory of Applied Chemistry of Chongqing Municipality, Institute of Bioorganic and Medicinal Chemistry, Southwest University, 400715, China.
E-mail address: liudf2009@swu.edu.cn (D. Liu).

https://doi.org/10.1016/j.bios.2019.03.016
Received 6 November 2018; Received in revised form 6 March 2019; Accepted 8 March 2019
Available online 09 March 2019
0956-5663/

of human total 3,3′,5-triiodothyronine with a high sensitivity (Feng et al., 2014). As compared to TPA, PLL has better biological compatibility owing to its amino acid units. It's worthy to mentioned that TPA is most commonly used as a co-reactant of $Ru(bpy)_3^{2+}$. Inspired by those, we propose a novel ECL sensor for improving the detection sensitivity of the luminol ECL system based on PLL as co-reactants.

Recently, polyluminol (PL) have been studied widely, for the reason that it can form PL film on graphite, glassy carbon, platinum, gold, screen printed and indium tin oxide electrodes to avoid conventional luminophore addition (Li et al., 2010). However, pure PL film has poor electroactivity, which limits its application in ECL detection. Polyaniline (PANI), the most promising materials, has lots of merits such as high conductivity, good stability, environmental friendship and biocompatibility (Inzelt et al., 2000; Zhang and Wang, 2006). The copolymer films of poly(luminol/aniline) (PLA) were performed on the electrode surface, provided better properties than the pure PL film (Ferreira et al., 2008; Liu et al., 2013). However, the loading of PLA nanorods on the electrode is low due to its large nanometer-size structure (Xiao et al., 2014). Reduced Graphene oxide (rGO), a single-layered two-dimensional sheet, can be used as versatile nanoscale building blocks to design a series of novel graphene-based nanocomposite (Cao et al., 2015; Kong et al., 2012; Yang et al., 2014; Wang et al., 2018b). Herein, Reduced graphene oxide (rGO) is used as a template to in situ grow PLA nanorods via π-π stacking and hydrogen bond interaction (Li et al., 2016). Due to high specific surface area, rGO could load amount of PLA. Thus, the PLA@rGO nanocomposite provided an enhanced ECL emission compared with individual PLA.

In this study, a novel ECL sensor platform based on PLA as ECL labels and PLL as co-reactant has been fabricated for the quantitative detection of GSH. Notably, the PLA@rGO in the detection solution containing PLL exhibited an enhanced ECL response (~5-fold) as compare to the solution without PLL because the PLL containing many amino groups could act as the co-reactant to significantly enhance the ECL of luminol. To the best of our knowledge, it is the first time that PLL was used for the co-reactant of luminol. The proposed ECL sensing platform was found to exhibit high sensitivity for the detection of GSH in the working solution. Scheme 1 shows the principle of ECL sensor platform for GSH detection. PLL could surprisingly and obviously enhance ECL intensity of luminol, however, as a typical free radical scavenger, GSH has great inhibitory effect on ECL of luminol. The as-prepared ECL sensor is simple, fast, high sensitivity, wide linear range and has a great potential application prospects in the way of monitoring and clinical diagnostics of GSH related diseases.

2. Experimental

2.1. Chemicals and reagents

Luminol and Glucose were bought from Macklin Biochemical Co. Ltd. (Shanghai, China). GSH (reduced form) and Graphene oxide were purchased from Aladdin and J&K Scientific Ltd. (Beijing, China). Poly-L-lysine hydrobromide (PLL, Mw = 30,000–70,000) was from Shanghai Yuanye Biotechnology Co. Ltd. (Shanghai, China). Poly(diallyldimethylammonium chloride) (PDDA, 20 wt%) was purchased from Sigma-Aldrich (St. Louis, MO, USA). KCl, $NaHCO_3$, Na_2CO_3, $CaCl_2$, Na_2SO_4, $Cu(NO_3)_2$, $Fe_2(SO_4)_3$, Ascorbic acid, Hydrazine hydrate ($N_2H_4{\cdot}H_2O$), Aniline and Ammonium persulphate ($(NH_4)_2S_2O_8$) were obtained from Taixin Reagent Company (Chongqing, China). L-cysteine, Serine, Glycine and Arginine were bought from Shanghai Taitan technology Co. Ltd. (Shanghai, China). All reagents were used without further purification. Double distilled water was used throughout all experiments.

2.2. Apparatus

ECL signals were recorded on a MPI-E multifunctional electrochemical and chemiluminescent analytical system (Remax Electronic Instrument Limited Co., Xi'an, China) and the voltage of the photomultipliter tube (PMT) was set at 700 V. The experiments were carried out with a conventional three-electrode system: a modified glassy carbon electrode (GCE) with 4 mm diameter as the working electrode, a platinum wire as the counter electrode and saturated calomel electrode (SCE) as the reference electrode. Cyclic voltammetry (CV) and electrochemical impedance spectroscopy (EIS) were collected on a CHI 604 electrochemical workstation (Chenhua, Shanghai, China). The thickness of rGO was investigated with atomic force microscope (AFM, Burker multimode 8). Scanning electron microscope (SEM) images were performed on a field emission-scanning electron microscope (FE-SEM, SU8020, Hitachi, Japan). The UV-vis absorption spectra were obtained on Shimadzu UV-3600 UV-vis-NIR photospectrometer (Shimadzu Co., Japan) at room temperature. The Fourie-transform infrared spectroscopy (FT-IR) was record on a TENSOR37 FT-IR spectrophotometer (Germany) using KBr pellets.

2.3. Preparation of rGO

The synthesis of rGO was performed according to the literature (Bai et al., 2012): in brief, 10 mL stable dispersion of graphene oxide (GO)

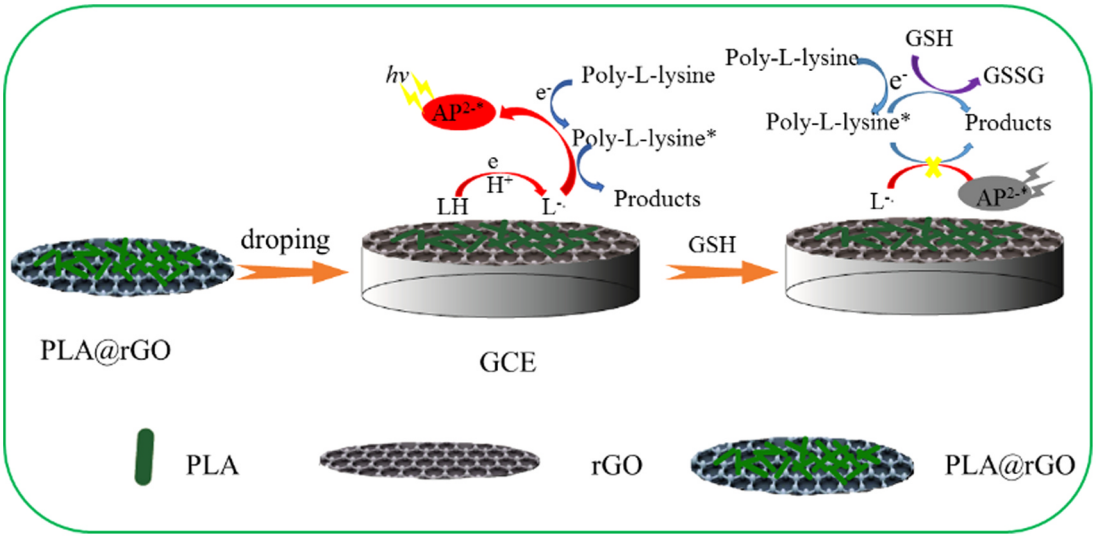

Scheme 1. Schematic principle of ECL sensor for GSH detection using PLL as co-reactant.

sheets (0.5 mg/mL) was mixed with 0.030 mL PDDA (20 wt%) stirred at room temperature for 30 min, then 50 μL of hydrazine hydrate was added and the mixture stirred in 90 °C water bath for 12 h. Finally, the rGO centrifuged and washed several times with double distilled water then redispersed in distilled water.

2.4. Synthesis of PLA@rGO and PLA

The PLA@rGO composite was prepared according to previous literature with some modifications (Xiao et al., 2014). Generally, 0.17 mL aniline and 0.0177 g luminol were added into 15 mL black dispersion of rGO nano-sheets and stirred vigorously at room temperature for 0.5 h, and cooled in an ice bath, After merged it with another 15 mL of pre-cooled 4.0 millimoles ammonium persulfate (APS) aqueous solution, and allowed to react at 0–5 °C for 12 h, the color of mixture solution changes from black to green black. The precipitates were collected, washed several times and vacuum dried at room temperature for 24 h. For comparison, PLA was also synthesized in the same way.

2.5. Construction of ECL biosensor

The glassy carbon electrode (GCE) was polished with 0.3 and 0.05 μm alumina slurry, followed by sonication in water, ethanol (v:v = 1:1), nitric acid (v:v = 1:1) and water sequentially and drying under room temperature. First, 2.0 mg PLA@rGO composite was dispersed into 1.0 mL of N, N-dimethylformamide (DMF) to form a uniform suspension. Then 4 μL of the PLA@rGO suspension was dropped on the GCE, and after drying in the room temperature, 4 μL of nafion solution (0.05 wt%) was dropped on it, and drying at the same condition.

2.6. ECL detection of GSH

The ECL signals were recorded using a MPI-E electrochemiluminescence analyzer in 2.5 mL 0.2 M CBS (pH 9.25) buffer containing 0.1 mg/mL PLL and different concentration of GSH. The voltage of the photo- multiplier tube (PMT) was set at 700 V and the applied potential was 0.1–0.9 V (vs. Ag/AgCl) with a scan rate of 100 mV/s in the process of detection.

3. Results and discussion

3.1. Characterization of rGO nanosheet, PLA nano-rod and PLA@rGO composite

The surface topographies and thickness of as-prepared rGO was determined by an AFM in tapping mode (Fig. S1A). A flake-like nanostructure was clearly observed and the average thickness of rGO was about 2–2.5 nm (Fig. S1B), indicating the formation of layered rGO. This is consistent with results reported in previous literature (Zhang et al., 2014a). More detailed structure was performed via SEM. The surface of rGO is fairly smooth and the wrinkled structure can be observed clearly (Fig. 1A). It can be seen that the prepared PLA presented a form of nanorod (Fig. 1B), which is similar to the reported structure in the literature (Xiao et al., 2014). A substantial amount of nanorods were intricately attached to the surface of rGO to make it very rough (Fig. 1C) and Fig. 1D was a magnified image showing the nanorods occupying the graphene surface, which indicated that PLA@rGO nanocomposite was prepared successfully.

The UV–vis spectra can provide more information to confirm the conjugate structure of nanocomposite. As shown in the Fig. S2 A, a wide absorption peak of rGO at 270 nm (curve a) assigned to π–π* transition of C=C (Li et al., 2015). PLA displayed three optical absorption spectra at 221, 312, and 350 nm (curve b) in which the absorption peak at 221 nm ascribed to the amino π-π* transition, and the absorption peaks at 312 and 350 nm ascribed to the n-π* transition (Liu et al., 2019). Three peaks at 221, 301, and 349 nm were observed with PLA@rGO resulting from overlapping of PLA and rGO spectra (curve c). The detailed reasons for the three peaks in composite are summarized as follows: When rGO mixed with PLA through π-π stacking interaction, π-electron delocalization of aromatic ring was promoted by the electron interaction in PLA@rGO, leading to red-shift of absorption peak in rGO. The red-shift peak overlaps with absorption peak at 312 nm to form another absorption peak at 301 nm.

FT-IR was also carried out to study rGO, PLA and PLA@ rGO, shown in Fig. S2 B, the FT-IR spectrum of rGO (Fig. S2 B, curve a) illustrates a broad peak at 3432 cm^{-1} owing to the stretching vibration of O-H. The peaks at 1629 and 1537 cm^{-1} could be assigned to C=C (aromatic ring) stretching vibration and the absorption band at 824 cm^{-1} be ascribed to C-H (aromatic ring) Out-of-plane bending vibration. Compared with GO, other absorption peaks of oxygen functionalities almost disappeared (C=O, epoxy groups, etc.), which indicated that the rGO has been successfully reduced. The FT-IR spectra of PLA (Fig. S2 B, curve b) shows that C=O stretching at around 1653 cm^{-1}, quinonoid and benzenoid ring vibration at 1557 and 1485 cm^{-1}, C-N stretching at 1297 $cm^{-1}$and N-H wag vibration at 802 cm^{-1} (Li et al., 2014). However, no carbonyl characteristic peaks were found in the FT-IR spectra of PLA@ rGO (Fig. S2 B, curve c) hybrid material. In addition, quinonoid and benzenoid ring vibration of composite red shifted to 1580 and 1497 cm^{-1}. This may be due to the interaction between the rGO and PLA, which results in a red shift and the disappearance of carbonyl peaks.

3.2. Electrochemical characterization of the proposed biosensor

The process of electrode modification was investigated via cyclic voltammetric (CV). Fig. S3 A reveals the CVs of the modification processes in the solution containing 10.0 mM $K_3[Fe(CN)_6]/K_4[Fe(CN)_6]$ (1:1) and 0.1 M KCl. Fig. S3 A illustrated that rGO and PLA exhibited excellent conductivity compared with bare GCE (curve a). At the same time, PANI provided much better conductivity than rGO, thus the peak current of PLA/GCE (curve c) was almost twice as high as rGO/GCE (curve b). However, after PLA was combined with rGO, the peak current of composite decreased relative to PLA, increased relative to rGO (curve d), indicating that the PLA@rGO composite has been prepared successfully. Although the introduction of PLA nanorods onto the surface of the rGO led to a decrement of conductivity, rGO could load a large amount of PLA nanorods owing to the high surface area.

Moreover, Consistent results were also achieved with the EIS (Fig S3 B) by monitoring the interface change of electron-transfer resistance (Ret). After the bare electrode were modified with rGO (curve b) and PLA (curve c), the Ret decreased obviously, which were attributed to the electron-promoting effect of PANI and rGO. It is clear that PLA exhibited a better conductivity than rGO, because a smaller semicircle domain was observed than rGO. When PLA@rGO was modified on electrode (curve d), a small Ret was observed. The Ret was smaller than rGO but larger than PLA, illustrating that PLA@rGO composite has been prepared successfully.

3.3. The ECL characterization of the amplified strategy

The ECL characterization was performed to confirm the value of rGO in the nanocomposite. An obviously enhancement ECL intensity could be observed using PLA@rGO (Fig. 2A, curve a) compared with individual PLA (Fig. 2A, curve b), which was mainly attributed to the large surface area of rGO. Although the conductivity of rGO was lower than PANI, rGO could support amount of PLA owing to the high surface area. Furthermore, the ECL response was also used to further confirm the amplified strategy. Almost no ECL intensity was observed at bare GCE (Fig. 2B, curve a), which could be ascribed to the lack of luminescence reagent. However, the PLA@rGO/GCE showed obvious ECL emission (Fig. 2B, curve c), which indicated the ECL signal originated from PLA@rGO. Furthermore, when co-reactant PLL was added into

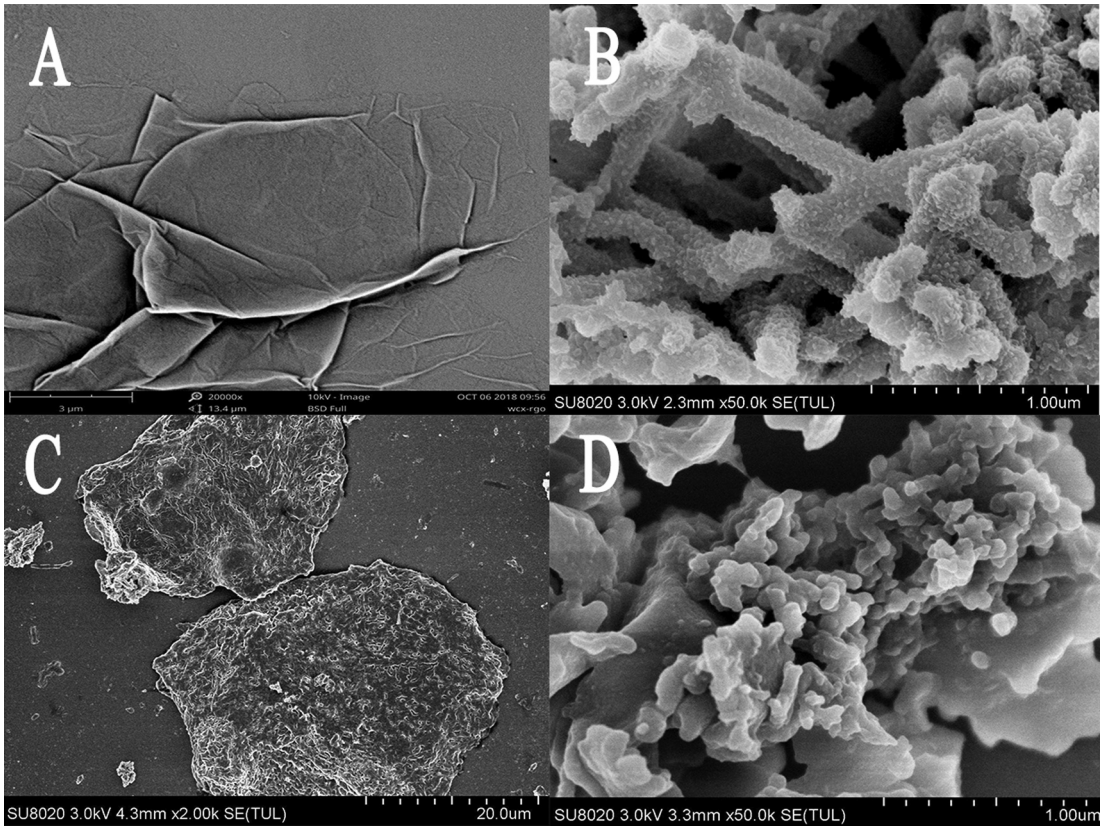

Fig. 1. SEM images of rGO (A), PLA (B) and PLA@rGO (C, D).

detection solution (Fig. 2B, curve b), the PLA@rGO/GCE exhibited an enhanced ECL response (~5-fold) as compare to absence of PLL, which demonstrated that PLL could significantly improve the ECL signal of luminol. The results above implied the formation of excellent ECL system, PLA@rGO/PLL, where the PLA were the ECL species and PLL acted as the co-reactant. Yuan and co-workers have reported that poly-L-lysine is amine oxidized in the presence of $Ru(bpy)_3^{2+}$ and then poly-L-lysine* can oxidize $Ru(bpy)_3^{3+}$ to produce $Ru(bpy)_3^{2+*}$ (Liao et al., 2013). Therefore, one possible ECL mechanism of luminol/poly-L-lysine ECL is that poly-L-lysine is amine oxidized to poly-L-lysine* and then poly-L-lysine* oxidizes $L^{\bullet-}$ (luminol radical anion) to AP^{2-*}, which emits light when it decays to its ground state.

$$LH - H^+ \rightarrow L^- \quad (1)$$

$$L^- - e \rightarrow L^\bullet \quad (2)$$

$$L^\bullet - H^+ \rightarrow L^{\bullet-} \quad (3)$$

$$\text{Poly-L-lysine} - e^- \rightarrow [\text{Poly-L-lysine}]^{*+} \rightarrow \text{Poly-L-lysine}^* + H^+ \quad (4)$$

$$L^{\bullet-} + \text{Poly-L-lysine}^* \rightarrow AP^{2-*} + \text{prouducts} \quad (5)$$

$$AP^{2-*} \rightarrow AP^{2-} + hv \quad (6)$$

As we all know, GSH is a common antioxidant and scavenger of free radicals due to its sulfhydryl groups. Nevertheless, poly-L-lysine* is a strong radical oxidant produced by poly-L-lysine. Thus, when a certain concentration of GSH was added to the detection solution, GSH could exhibit antioxidant properties, it reacted with poly-L-lysine* quickly, which led to a significant decreasing of anode ECL emission of PLA@rGO/GCE (Fig. 2B, curve d). GSH competed with luminol for the reactive sites of poly-L-lysine*, which limited that poly-L-lysine* oxidizes $L^{\bullet-}$ (luminol radical anion) to AP^{2-*}, resulting in a weak ECL intensity of luminol (Scheme 1).

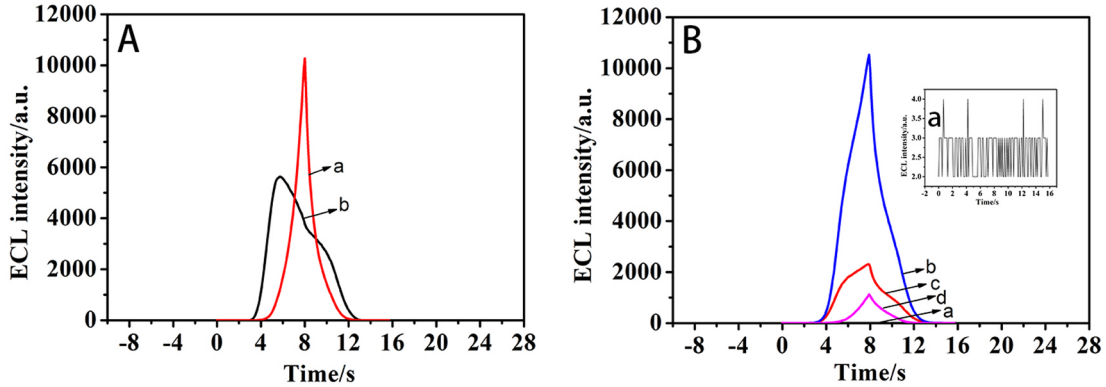

Fig. 2. (A) ECL behaviors of PLA@rGO (a) and PLA (b) in 0.2 M CBS buffer solution (pH 9.25) with 0.1 mg/mL PLL. (B) ECL-time curves of bare GCE (a), PLA@rGO (b), PLA@rGO with 0.1 mg/mL PLL(c), PLA@rGO with 0.1 mg/mL PLL and 1.0 mM GSH (d) in 0.2 M CBS buffer solution (pH 9.25).

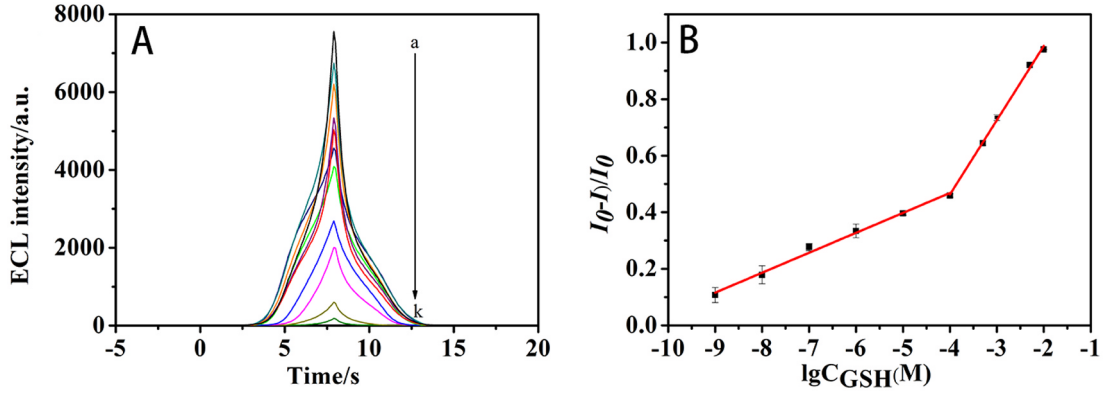

Fig. 3. ECL-time curves of proposed sensor at different GSH concentrations (a–k: 0, 1.0×10^{-9}, 1.0×10^{-8}, 1.0×10^{-7}, 1.0×10^{-6}, 1.0×10^{-5}, 1.0×10^{-4}, 0.5×10^{-3}, 1.0×10^{-3}, 0.5×10^{-2}, and 1.0×10^{-2} M, respectively) (A). Calibration curves of GSH detection (B).

$$\text{Poly-L-lysine}^{*} + \text{GSH} + \text{OH}^{-} \rightarrow \text{GS-SG} + \text{prouducts} + \text{H}_2\text{O} \quad (7)$$

3.4. Optimization of experimental conditions

In order to obtain a high-performance ECL biosensor, a single variable method was used to optimize the conditions of bioassay, including the pH of detection solution, the concentration of co-reactant (PLL) and the modification quantity of material. I and I_0 were chosen as the ECL intensity of in presence and absence of GSH, and $(I_0 - I)/ I_0$ is the ECL inhibition efficiency. As shown in Fig. S4 A, the ECL inhibition efficiency enhanced with an increase of pH and reached the maximum value at pH of 9.25, and then decreased. Therefore, pH of 9.25 CBS was adopted as the optimal value for all subsequent experiments and determination of real sample. The concentration of PLL also is an important factor for co-reactant ECL system. The ECL emission efficiency improved with the increasing concentration of PLL and appeared the maximum at the concentration of 0.1 mg/mL (Fig. S4 B), which may be due to the fact that PLL is easily decomposed and denatured in a strong alkaline solution. Moreover, the decomposition velocity of PLL becomes fast when the concentration increases. Thus, we choose 0.1 mg/mL as the optimum concentration of PLL in GSH sensing experiments. Fig. S4C shows the effect of modification quantity of PLA@rGO. The ECL signal increased significantly as the increase of the amount of modification, then declined sharply when the loading mass of PLA@rGO is more than 4 μL. Therefore, 4 μL was selected as the applied modification quantity in the subsequent ECL sensing experiments.

3.5. Selectivity of the ECL biosensor in GSH detection

The selectivity of the ECL sensor was investigated through measurement of its responses to other amino acids, mental ions, anions and biomolecules (i.e., serine (Ser), arginine (Arg), glycine (Gly), cysteine (Cys), ascorbic acid (AA), glucose (Glu), Na_2SO_4, KCl, $CaCl_2$, $Cu(NO_3)_2$, $Fe_2(SO_4)_3$). The ECL inhibition efficiency of GSH is much higher than other substance, such as ascorbic acid, amino acids, ions and glucose (Fig. S4 D). High concentrations of cysteine (Cys) also can weak ECL intensity, however, their concentrations (micromolar levels) is very low in the biological systems (Cai et al., 2015; Yu et al., 2013). Therefore, this method could be used for selective GSH detection.

3.6. Analytical performance of proposed ECL biosensor

The analytical performance of the PLA@rGO-based ECL sensor for GSH detection was evaluated by adding various concentrations of GSH to detection solution (Fig. 3A). A good linear relationship between the ECL inhibition efficiency ($(I_0 - I)/ I_0$) and the logarithm of concentration of GSH (log c) were achieved in the ranges of 1.0×10^{-9}–1.0×10^{-4} M and 1.0×10^{-4}–1.0×10^{-2} M with a limit of detection (LOD) of 0.77 nM (S/N = 3). The homologous linear equation were $(I_0 - I) /I_0 = 0.75 + 0.070 \log$ (C/M) (R = 0.991) and $(I_0 - I) /I_0 = 1.51 + 0.262 \log$ (C/M) (R = 0.997), respectively (Fig. 3B). It can be seen that the proposed ECL sensor in this work displays a wide linear range response and low detection limit based on a comparison study between this work and previously reported GSH sensing methods (Table 1). Thus, the proposed ECL sensor not only expands the application of the PLA@rGO -based ECL sensing platform but also provides a new field for the rapid and sensitive detection of GSH.

3.7. GSH detection in human serum samples

The performance of prepared ECL sensor in real sample analysis was investigated via detecting GSH concentration in fresh human serum. The fresh serum was diluted 100 times so that GSH concentration was within the linear range of the assay and then the diluted human serum samples were utilized to the recovery tests. A certain amount of GSH

Table 1
Comparison of different methods for GSH detection.

Method	Probes	Liner range (M)	LOD (M)	References
SERS	AuF/MP	1.17×10^{-6}–1.9×10^{-5}	1.4×10^{-7}	Wang et al. (2016)
Colorimetry	Ag^{+}-TMB	5.0×10^{-8}–8.0×10^{-6}	5.0×10^{-8}	Ni et al. (2015)
Colorimetry	Fe_3O_4/MIL-88-H_2O_2-MB	0–0.55×10^{-6}, 0.55×10^{-6}–3.0×10^{-6}	3.69×10^{-8}	Zhang et al. (2018)
Colorimetry	MnO_2 NS-TMB	1.0×10^{-6}-2.5×10^{-5}	3.0×10^{-7}	Liu et al. (2017)
Electrochemistry	$Cu(OH)_2$-CILE	1.0×10^{-6}–5.0×10^{-5};1.0×10^{-4}–1.8×10^{-3}	3.0×10^{-8}	Safavi et al. (2009)
Fluorescence	MnO_2 NS	2.0×10^{-8}–2.0×10^{-6}	6.7×10^{-9}	Fan et al. (2017)
Fluorescence	MnO_2 NS upconversion nanoparticles	Not given	0.9×10^{-6}	Deng et al. (2011)
Fluorescence	g-C_3N_4/MnO_2	Not given	0.2×10^{-6}	Zhang et al. (2014b)
ECL	Lucigenin/MnO_2	1×10^{-8}–2×10^{-6}	3.7×10^{-9}	Gao et al. (2016)
ECL	GO/CdTe QDs	2.4×10^{-5}–2.14×10^{-4}	8.3×10^{-6}	Wang et al. (2009)
ECL	PLA@rGO/GCE	1.0×10^{-9}–1.0×10^{-4}, 1.0×10^{-4}–1.0×10^{-2}	7.7×10^{-10}	This work

was spiked into the serum samples. The acceptable recoveries in the range of 99.9–100.3% were obtained by spiking low concentration GSH (Table S1). Furthermore, the recoveries range from 97.9% to 105.0% when high concentration GSH was spiked (Table S2). These reasonable recoveries indicate the satisfactory applicability of this ECL sensor in human serum samples.

4. Conclusion

In conclusion, PLL was proposed for the first time as a novel and efficient co-reactant of the luminol system to enhance ECL and confirmed by ECL spectra. Furthermore, a 5-fold enhancement was observed compared with individual PLA@rGO modified on GCE. However, GSH could compete with luminol for the reactive of PLL and obviously inhibit the ECL of luminol. Inspired by this, an ultrasensitive ECL biosensor was constructed for the GSH detection using PLL as a novel co-reactant of luminol. Besides, the prepared ECL sensor exhibited a high sensitivity and wide dynamic range for detection of GSH in human serum sample. This work would open a new filed where compound containing active amino functional groups would be used as a novel co-reactant of luminol.

Acknowledgments

We sincerely acknowledge the financial support of the National Natural Science Foundation of China (No. 61503309), and the Fundamental Research Funds for the Central Universities (XDJK2015C019) and the Dr. Start-up Foundation of the Southwest University (SWU113074).

Credit author statement

All authors have given approval to the final version of the manuscript and these authors contributed equally to this work.

Declaration of interests

None.

Appendix A. Supporting information

Supplementary data associated with this article can be found in the online version at doi:10.1016/j.bios.2019.03.016.

References

Bai, L.J., Yuan, R., Chai, Y.Q., Yuan, Y.L., Wang, Y., Xie, S.B., 2012. Chem. Commun. 48, 10972–10974.
Cai, Q.Y., Li, J., Ge, J., Zhang, L., Hu, Y.L., Li, Z.H., Q, L.B., 2015. Biosens. Bioelectron. 72, 31–36.
Cao, X., Gao, J., Ye, Y.P., Ding, S., Ye, Y., Sun, H., 2015. Electroanalysis 27, 1–6.
Cao, Y.L., Yuan, R., Chai, Y.Q., Mao, L., Niu, H., Liu, H.J., Zhuo, Y., 2012. Biosens. Bioelectron. 31, 305–309.
Deng, R., Xie, X., Vendrell, M., Chang, Y.T., Liu, X., 2011. J. Am. Chem. Soc. 133, 20168–20171.
Fan, D.Q., Shang, C.S., Gu, W.L., Wang, E.K., Dong, S.J., 2017. ACS Appl. Mater. Interfaces 9, 25870–25877.
Feng, X., Gan, N., Zhou, J., Li, T.H., Cao, Y.T., Hu, F.T., Yu, H.W., Jiang, Q.L., 2014. Electrochim. Acta 139, 127–136.
Ferreira, V., Cascalheira, A.C., Abrantes, L.M., 2008. Electrochim. Acta 53, 3803–3811.
Gao, W., Liu, Z., Qi, L., Wu, L.J., Zheng, A., Wu, L., Zhang, X., 2016. Anal. Chem. 88, 7654–7659.
Haghighi, B., Bozorgzadeh, S., 2011. Anal. Chim. Acta 697, 90–97.
Hanif, S., Han, S., John, P., Gao, W., Kitte, S.A., Xu, G., 2016. Electrochim. Acta 196, 245–251.
Harfield, J.C., Batchelor-McAuley, C., Compton, R.G., 2012. Analyst 137, 2285–2296.
Inzelt, G., Pineri, M., Schultze, J.W., Vorotyntsev, M.A., 2000. Electrochim. Acta 45, 2403–2421.
Kong, F.Y., Li, X.R., Zhao, W.W., Xu, J.J., Chen, H.Y., 2012. Electrochem. Commun. 14, 59–62.
Li, G.X., Lian, J.L., Zheng, X.W., Cao, J., 2010. Biosens. Bioelectron. 26, 643–648.
Li, L.L., Chen, Y., Zhu, J.J., 2017. Anal. Chem. 89, 358–371.
Li, L.L., Liu, K.P., Yang, G.H., Wang, C.M., Zhang, J.R., Zhu, J.J., 2015. Adv. Funct. Mater. 21, 869–878.
Li, X., Zhang, C.F., Xin, S., Yang, Z.C., Li, Y.T., Zhang, D.W., Yao, P., 2016. ACS Appl. Mater. Interfaces 8, 21373–21380.
Li, Z.F., Zhang, H.Y., Liu, Q., Liu, Y.D., Stanciu, L., Xie, J., 2014. Carbon 71, 257–267.
Liao, N., Zhuo, Y., Chai, Y.Q., Xiang, Y., Han, J., Yuan, R., 2013. Biosens. Bioelectron. 45, 189–194.
Liu, C., Wei, X.H., Tu, Y.F., 2013. Talanta 111, 156–162.
Liu, J., Meng, L.J., Fei, Z.F., Dyson, P., Jing, X.N., Liu, X., 2017. Biosens. Bioelectron. 90, 69–74.
Liu, W., Chen, A.Y., Li, S.K., Peng, K.F., Chai, Y.Q., Yuan, R., 2019. Anal. Chem. 91, 1516–1523.
Liu, Z., Qi, W., Xu, G., 2015. Chem. Soc. Rev. 44, 3117–3142.
Ni, P.J., Sun, Y.J., Dai, H.C., Hu, J.T., Jiang, S., Wang, Y.L., Li, Z., 2015. Biosens. Bioelectron. 63, 47–52.
Peng, H.P., Jian, M.L., Huang, Z.N., Wang, W.J., Deng, H.H., Wu, W.H., Liu, A.L., Xia, X.H., Chen, W., 2018. Biosens. Bioelectron. 105, 71–76.
Safavi, A., Maleki, N., Farjami, E., Mahyari, F.A., 2009. Anal. Chem. 81, 7538–7543.
Stamler, J.S., Slivka, A., 1996. Nutr. Rev. 54, 1–30.
Sun, X.L., Wang, H., Jian, Y.N., Lan, F.F., Zhang, L.N., Liu, H.Y., Ge, S.G., Yu, J.H., 2018. Biosens. Bioelectron. 105, 218–225.
Wang, H., Jian, Y.N., Kong, Q.K., Liu, H.Y., Lan, F.F., Liang, L.L., Ge, S.G., Yu, J.H., 2018a. Sens. Actuators B. 257, 561–569.
Wang, H., Zhou, C.X., Sun, X.L., Jian, Y.N., Kong, Q.K., Cui, K., Ge, S.G., Yu, J.H., 2018b. Biosens. Bioelectron. 117, 651–658.
Wang, W.K., Zhang, L.M., Li, L., Tian, Y., 2016. Anal. Chem. 88, 9518–9523.
Wang, Y., Lu, J., Tang, L., Niu, S., 2009. Anal. Chem. 81, 9710–9715.
Xiao, C.B., Zhao, Q., Tu, Y.F., 2014. Electrochim. Acta 147, 791–796.
Xu, G.F., Zeng, X.X., Lu, S.Y., Gong, L.S., Lin, Y.Y., Wang, Q.P., Tong, Y.J., Chen, G.N., 2013. Luminescence 28, 456–460.
Yang, Z.T., Qian, J., Yang, X.W., Jiang, D., Du, X.J., Wang, K., Mao, H., Wang, K., 2014. Biosens. Bioelectron. 65, 39–46.
Yin, J., Kwon, Y., Kim, D., Lee, D., Kim, G., Hu, Y., Yoon, J., 2014. J. Am. Chem. Soc. 136, 5351–5358.
Yu, F.B., Li, P., Wang, B.S., Han, K., 2013. J. Am. Chem. Soc. 135, 7674–7680.
Zhang, D.H., Wang, Y.Y., 2006. Mater. Sci. Eng B. 134, 9–19.
Zhang, J.J., Wang, W.T., Chen, S.H., Yuan, R., Zhong, X., Wu, X.P., 2014a. Biosens. Bioelectron. 57, 71–76.
Zhang, X.L., Zheng, C., Guo, S.S., Li, J., Yang, H.H., Chen, G.N., 2014b. Anal. Chem. 86, 3426–3434.
Zhang, Y., Zhang, W.T., Chen, K., Yang, Q.F., Hu, N., Suo, Y.R., Wang, J.L., 2018. Sens. Actuators B. 262, 95–101.